The Role of Metal Ion Dopants in Quantum-Sized TiO2: Correlation Between Photoreactivity and Charge Carrier Recombination Dynamics

ARTICLE *in* THE JOURNAL OF PHYSICAL CHEMISTRY · DECEMBER 1994

Impact Factor: 2.78 · DOI: 10.1021/j100102a038

3 AUTHORS:

Wonyong Choi
Pohang University of Science and Technology
256 PUBLICATIONS **23,408** CITATIONS
SEE PROFILE

Andreas Termin
Vertex Pharmaceuticals, United States, San D…
24 PUBLICATIONS **2,429** CITATIONS
SEE PROFILE

Michael R. Hoffmann
California Institute of Technology
377 PUBLICATIONS **29,836** CITATIONS
SEE PROFILE

The Role of Metal Ion Dopants in Quantum-Sized TiO_2: Correlation between Photoreactivity and Charge Carrier Recombination Dynamics

Wonyong Choi, Andreas Termin, and Michael R. Hoffmann*

W. M. Keck Laboratories, California Institute of Technology, Pasadena, California 91125

Received: July 15, 1994; In Final Form: October 12, 1994[⊗]

A systematic study of metal ion doping in quantum (Q)-sized (2−4 nm) TiO_2 colloids is performed by measuring their photoreactivities and the transient charge carrier recombination dynamics. The presence of metal ion dopants in the TiO_2 crystalline matrix significantly influences photoreactivity, charge carrier recombination rates, and interfacial electron-transfer rates. The photoreactivities of 21 metal ion-doped colloids are quantified in terms of both the conduction band electron reduction of an electron acceptor (CCl_4 dechlorination) and the valence band hole oxidation of an electron donor ($CHCl_3$ degradation). Doping with Fe^{3+}, Mo^{5+}, Ru^{3+}, Os^{3+}, Re^{5+}, V^{4+}, and Rh^{3+} at 0.1−0.5 at. % significantly increases the photoreactivity for both oxidation and reduction while Co^{3+} and Al^{3+} doping decreases the photoreactivity. The transient absorption signals upon laser flash photolysis (λ_{ex} = 355 nm) at λ = 600 nm are extended up to 50 ms for Fe^{3+}-, V^{4+}-, Mo^{5+}-, and Ru^{3+}-doped TiO_2 while the undoped Q-sized TiO_2 shows a complete "blue electron" signal decay within 200 μs. Co^{3+}- and Al^{3+}-doped TiO_2 are characterized by rapid signal decays with a complete loss of absorption signals within 5 μs. The quantum yields obtained during CW photolyses are quantitatively correlated with the measured transient absorption signals of the charge carriers. Photoreactivities are shown to increase with the relative concentration of trapped charge carriers. The photoreactivity of doped TiO_2 appears to be a complex function of the dopant concentration, the energy level of dopants within the TiO_2 lattice, their d electronic configuration, the distribution of dopants, the electron donor concentration, and the light intensity.

Introduction

TiO_2 photocatalysis has been the focus of numerous investigations in recent years,[1] particularly because its application for the quantitative destruction of undesirable chemical contaminants appears to be a promising process for water and air pollution control.[2] Complete mineralization of a wide variety of organic compounds to CO_2, H_2O, and inorganic constituents has been reported.[1a] Photocatalytic efficiency of TiO_2 depends, in part, upon the relative degree of branching of the reactive electron/hole pairs into interfacial charge-transfer reactions. In order to enhance interfacial charge-transfer reactions, the properties of TiO_2 colloids and electrodes have been modified by selective surface treatments such as surface chelation,[3] surface derivatization,[4] and platinization[5] and by selective metal ion doping[6−20] of the crystalline TiO_2 matrix.

Several transition metal ion dopants in TiO_2 have been investigated previously. Fe^{3+} was shown to increase the efficiency of photoreduction of N_2[8,10] and methyl viologen[6] and to inhibit electron/hole pair recombination in TiO_2.[7b] In the case of the photodegradation of phenol, Fe^{3+} doping of TiO_2 had little effect on relative photoreactivity.[10] Enhanced photoreactivity for water cleavage[18] and N_2 reduction[10b] with Cr^{3+}-doped TiO_2 have been reported while other researchers have shown that Cr^{3+} was detrimental to the photocatalytic activity.[13c,15] TiO_2 doped with Mo and V exhibited significantly reduced photoactivity[14] although Grätzel and Howe[7a] suggested an inhibition of electron/hole pair recombination with these dopants based on EPR data. Mu et al.[15] reported that doping with trivalent or pentavalent metal ions was detrimental to the photocatalytic reactivity while Karakitsou and Verykios[16] showed that doping with cations of valency higher than that of Ti^{4+} enhanced photoreactivity.

Even though metal ion doping effects on the reactivity of TiO_2 have been a frequent topic of investigation, direct comparisons and unifying conclusions are difficult to make since widely-varying experimental conditions for sample preparation and for the determination of photoreactivity have been employed. Furthermore, there appears to be no direct correlation between the photophysical measurements[7] and photochemical reactivity.[10,15]

In this paper, we present a systematic study of metal ion doping of quantum (Q)-sized TiO_2 for 21 metal ions. On the basis of both photochemical and photophysical measurements, we offer a general explanation for the role of metal ion dopants in TiO_2 photocatalysis. The photoreactivities of doped Q-sized TiO_2 colloids (transparent particle suspensions) are quantified in terms of both the conduction band (CB) electron reduction of CCl_4 and the valence band (VB) hole oxidation of $CHCl_3$.[21] Measured photoreactivities for the doped TiO_2 colloids are compared with their photoexcited transient absorption spectra in order to probe the relationship between photoreactivity and charge pair recombination.

Experimental Section

Colloid Synthesis and Characterization. Q-sized TiO_2 colloids were prepared from the controlled hydrolysis of titanium tetraisopropoxide.[22] A 1.25 mL sample of $Ti(OCH(CH_3)_2)_4$ (Aldrich, 97%) dissolved in 25 mL of absolute ethanol was added dropwise under vigorous stirring to 250 mL of distilled water (4 °C) adjusted to pH 1.5 with nitric acid. The resulting transparent colloidal suspension (1.34 g/L) was stirred overnight. The colloidal suspension can be stored in a cold room (4 °C) for over 1 year without coagulation. To obtain powder sample, the above colloidal solution was evaporated (35 °C) using a rotavapor and dried under vacuum. The powdered sample contained ~30 wt % of HNO_3. Redissolving the powder in

* To whom correspondence should be addressed.

[⊗] Abstract published in *Advance ACS Abstracts*, December 1, 1994.

0022-3654/94/2098-13669$04.50/0

distilled water with 0.5 g of TiO_2/L resulted in a transparent suspension of pH 2.8 ± 0.1. The presence of nitrate in the TiO_2 samples may induce secondary photochemical effects because the direct photolysis of nitrate can result in the formation of hydroxyl radicals which directly initiate degradation reactions of organic substrates.[23] In order to assess this side effect from nitrate, a TiO_2 sample was prepared using perchloric acid instead of nitric acid under otherwise same conditions. No difference in the photocatalytic reactivity was found between the two TiO_2 samples.

Doped Q-sized TiO_2 was prepared according to the above procedure in the presence of added metal salts to give a doping level from 0.1 to 3.0 at.%. All the dopant concentrations mentioned in this work are the nominal atomic concentration which is based upon the assumption of quantitative incorporation of the dopant. All the available dopant metal ions which have an ionic radius similar to that of Ti^{4+} (0.75 Å) were chosen for substitution into the lattice. Metal salts used as precursors for dopant ions are listed as follows: LiOH, $Mg(ClO_4)_2$, $AlCl_3$, VCl_3, $VOSO_4 \cdot 3H_2O$, $VOCl_3$, $Cr(NO_3)_3$, MnF_3, $Fe(NO_3)_3 \cdot 9H_2O$, CoF_3, $NiCl_2$, $Zn(ClO_4)_2$, $Ga(NO_3)_3$, $Zr(OCH(CH_3)_2)_4$, $NbCl_5$, $MoCl_5$, $RuCl_3$, $Rh(NO_3)_3 \cdot 2H_2O$, $SnCl_4$, $SbCl_5$, $TaCl_5$, $ReCl_5$, and $OsCl_3$. Precursors of $Zr(OCH(CH_3)_2)_4$, $NbCl_5$, $SbCl_5$, and $TaCl_5$ were dissolved in ethanol along with titanium tetraisopropoxide while the others were added to the acidic water. Doped TiO_2 powder samples displayed various colors depending on the kind of metal ions and their concentrations: V^{3+}-, V^{4+}-, V^{5+}-, Fe^{3+}-, Rh^{3+}-, and Re^{5+}-doped samples were yellowish, Cr^{3+}-doped greenish, Co^{3+}-doped pink, Ni^{2+}-doped bright blue, Ru^{3+}-doped dark brown, and Mn^{3+}- and Os^{3+}-doped greenish to brownish gray. Inductively coupled plasma−mass spectrometry (ICP-MS) analysis of the supernatant from coagulated doped colloids showed no significant amount of dissolved metal ions.

The particle sizes were determined by a Philips EM 430 transmission electron microscope (TEM) at 300 kV. TEM samples were prepared on a copper mesh substrate covered with an amorphous carbon film. The particle sizes were 2−4 nm. A particle of 3 nm diameter consists of 410 TiO_2 monomers. Analysis of lattice fringes in an individual small particle showed the lattice spacing of 3.6 ± 0.1 Å, which is in good agreement with the anatase (101) lattice spacing of 3.51 Å. X-ray diffraction (XRD) and Raman spectroscopy analysis showed the presence only of the anatase as well. The line broadening in the diffractogram of Q-sized TiO_2 was analyzed by the Scherrer equation to give the particle sizes of 3−4 nm, which well matched the TEM analysis. UV−visible absorption spectra of various doped TiO_2 colloidal suspensions were recorded on a HP8451A diode array spectrophotometer.

Photoreactivity Measurements. The photoreactivity of each doped TiO_2 system was quantified in terms of $CHCl_3$ oxidation by VB holes (or trapped holes)[24]

$$CHCl_3 + h_{vb}^+ \ (>Ti^{IV}OH_s^{\bullet}) \rightarrow H^+ + CCl_3^{\bullet} \qquad (1)$$

and CCl_4 reduction by CB electrons (or trapped electrons)[25,28]

$$CCl_4 + e_{cb}^- \ (>Ti^{III}-OH_s^-) \rightarrow Cl^- + CCl_3^{\bullet} \qquad (2)$$

where h_{vb}^+ refers to a valence band hole, a trapped hole, or a surface-bound •OH radical and e_{cb}^- refers to a conduction band electron or a trapped electron. Reaction 2 was performed in the presence of added methanol (0.1 M) as a hole scavenger.

One complexity may arise in the CCl_4/CH_3OH system because methanol forms α-hydroxymethyl radicals upon the hole-initiated hydrogen atom abstraction which are strong one-electron reductants ($E_{1/2}(^{\bullet}CH_2OH/HCHO) = -0.74$ V vs NHE).[26] As a result, the α-hydroxymethyl radicals can directly reduce CCl_4 as follows:[27]

$$^{\bullet}CH_2OH + CCl_4 \rightarrow HCHO + CCl_3^{\bullet} + H^+ + Cl^-$$

$$k \leq 10^6\ M^{-1}\ s^{-1} \qquad (3)$$

The above reaction enables CCl_4 to be reduced by the hole-initiated pathway, which makes the assessment of photoreduction by CB electrons difficult. However, under the air-saturation condition of the present study, reaction 3 competes with the addition of molecular oxygen to the $^{\bullet}CH_2OH$ radical. Using the experimental conditions employed in this paper (vide infra) and the literature rate constants ($k(^{\bullet}CH_2OH+O_2) = 4.9 \times 10^9\ M^{-1}\ s^{-1}$),[27] we calculate that only 0.5% of the $^{\bullet}CH_2OH$ radicals proceed via reaction 3. In the recent study of CCl_4 photoreduction in TiO_2 suspensions,[28] we compared the efficiency of methanol as a hole scavenger with that of *tert*-butyl alcohol, which does not form α-hydroxyalkyl radicals; the dechlorination rate was only slightly higher in the CCl_4/methanol system than in the CCl_4/*tert*-butyl alcohol system under the same experimental conditions to this work.

Irradiation was performed with a 1000 W Xe arc lamp (Spindler and Hoyer). Light was filtered by a 10 cm IR water filter and a UV interference filter (Oriel) which transmitts light only at 320 ± 7 nm and was subsequently focused onto a reactor cell. The light intensity measurement was performed by chemical actinometry using (*E*)-α-(2,5-dimethyl-3-furylethylidene)(isopropylidene)succinic anhydride (Aberchrome 540).[29] Light intensity was varied using neutral density filters. In our experiments, the intrinsic quantum yield for each reaction was measured precisely since transparent colloidal suspensions, which exhibit negligible light scattering, were used. Both reactions 1 and 2 were followed by measuring the Cl^- production after 1 h of UV irradiation with an Orion chloride ion-selective electrode. Chloride production was linear over this time period (1 h). Chloride adsorption on the colloidal particles was found to be negligible under our experimental conditions. Solutions of desired organic substrate concentrations were prepared by dilution of the saturated stock solutions ($CHCl_3$, 63 mM; CCl_4, 5.1 mM). In a typical experiment, a glass reactor cell (35 mL) with a quartz irradiation window was filled to capacity, sealed tightly from the atmosphere, and irradiated with constant magnetic stirring. Reaction 1 was performed at pH 11.0 ± 0.2 with $[CHCl_3]_0 = 3.15$ mM. Colloidal suspensions at this basic pH were prepared without coagulation by fast addition of 1.0 N NaOH solution to a vigorously stirred acidic suspension. Reaction 2 was performed at pH 2.8 ± 0.1 with $[CCl_4]_0 = 5.1$ mM and $[CH_3OH]_0 = 0.1$ M. In both cases $[TiO_2] = 0.5$ g L^{-1}, $[O_2]_{diss} \approx 0.2$ mM (air equilibration), and $I = 1.28 \times 10^{-4}$ einstein L^{-1} min^{-1} (at 320 nm, full width at half-maximum 15 nm).

Transient Absorption Experiments. TiO_2 samples for the laser flash photolysis experiments were prepared using hydrochloric acid instead of nitric acid for a pH control in order to avoid the interference from the conduction band electron transfer to nitrate ions. Colloidal solutions of Q-sized TiO_2/HCl (1 g L^{-1}, pH 2.3 ± 0.2) were transferred into a vacuum cell having an 1.0 cm optical cuvette side arm. The samples were degassed under vacuum and purged with Ar on a vacuum/argon line. At least five vacuum/fill cycles were done to deoxygenate samples. The deoxygenated samples were excited with pulses from a Q-switched frequency-tripled Nd:YAG laser (355 nm, 10 ns fwhm). Excitation pulse energies were ~1.5 mJ/pulse (2.7×10^{15} photons/pulse). Single-wavelength transient absorption kinetics were observed using a 75 W Xe arc lamp (pulsed lamp

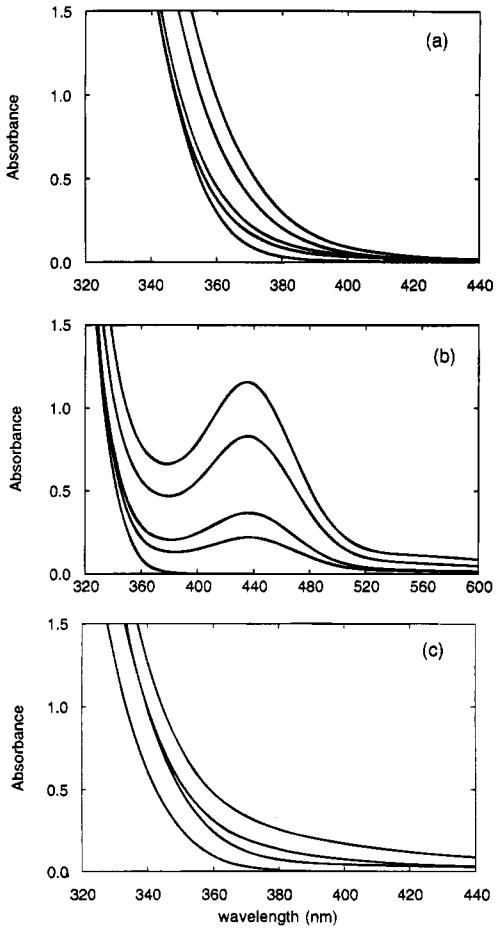

Figure 1. Absorption spectra of (a) Fe^{3+}-doped Q-sized TiO_2 (1.34 g/L) at 0.0, 1.0, 2.0, 5.0, and 10.0% Fe^{3+} concentrations (from left to right), (b) Ru^{3+}-doped Q-sized TiO_2 (0.5 g/L) at 0.0, 0.5, 1.0, 2.0, and 3.0% Ru^{3+} concentrations (from bottom to up), and (c) undoped, Rh^{3+} (3.0%), V^{4+} (3.0%), and Mn^{3+} (3.0%) Q-sized TiO_2 at 0.5 g/L (from left to right).

mode) as a probe source. All the decay kinetics were monitored by following the trapped charge carrier absorption at 600 nm. A detailed description of the experimental setup has been provided previously.[30]

Results

Absorption Spectra of Colloids. The band gap of the undoped Q-sized TiO_2 particles was determined to be 3.37 eV (369 nm) according to the spectral analysis described by Kormann et al.[22b] This corresponds to 0.17 eV blue shift from the bulk-phase band gap for anatase (3.2 eV). According to a theoretical prediction proposed by Brus[38]

$$\Delta E_g = \frac{h^2}{8R^2\mu} - \frac{1.8e^2}{\epsilon R} \quad (4)$$

(R, radius of the particle; μ, reduced mass of the exciton = $1.63m_e$ for TiO_2;[22b] ϵ, dielectric constant of the semiconductor = 184 for TiO_2[22b]) the bandgap shift of 0.17 eV in TiO_2 corresponds to a particle size of 2.2 nm, which well matches the particle size determined by TEM. Figure 1 shows the absorption spectra of some doped colloids. The spectra of Fe^{3+}-doped colloids show a red shift in the band gap transition with an increase in dopant concentration. This shift is consistent with the incorporation of the doping metal ions into the TiO_2 nanoparticles. V^{4+}, Rh^{3+}, and Mn^{3+} show similar band gap shifts. Red shifts of this type can be attributed to the charge-transfer transitions between the metal ion d electrons and the TiO_2 conduction or valence band.[7b,18] In the case of Ru^{3+}, which was incorporated into the TiO_2 lattice, a strong absorption band centered at 437 nm was observed. This band is not present in the spectrum of hexaaquo Ru^{3+} ions in solution. In addition, free hexaaquo Ru^{3+} ions have a fluorescence peak centered at 361 nm (λ_{ex} = 320 nm) while the Ru^{3+}-doped TiO_2 colloids do not exhibit fluorescence. This result is consistent with the incorporation of Ru^{3+} ions into the TiO_2 lattice. However, the Ru^{3+}-doped colloid exhibited no photoactivity for either oxidation or reduction with $\lambda > 390$ nm.

Photoreactivities of Doped Q-Sized TiO_2. The photoreactivities of doped Q-sized TiO_2 depend on the dopants and their concentrations. Table 1 lists the chloroform degradation quantum yields (percent) for several doped colloids as a function of dopant level. All dopants show an optimum concentration above which the observed quantum yields for $CHCl_3$ degradation decrease. The highest quantum yields are generally seen at 0.5%. The number of dopant ions per individual TiO_2 particle at the dopant concentration of 0.5 at. % is between one and five. Co^{3+}-doped TiO_2 shows a steady decrease in the Φ_{CHCl_3} with increasing the dopant concentration.

The measured photoreactivities of 21 doped Q-sized TiO_2 colloids are summarized in Figure 2 in terms of the observed quantum yield for $CHCl_3$ oxidation ($\Phi_{CHCl_3} = {}^1/_3\{(d[Cl^-]/dt)/I_a\}$) and for CCl_4 reduction ($\Phi_{CCl_4/Cl^-} = (d[Cl^-]/dt)/I_a$). Several dopants increase the photoreactivity significantly compared to the undoped Q-sized TiO_2. In order of decreasing reactivity they are Fe^{3+} (15-fold), Mo^{5+} (11-fold), Ru^{3+} (11-fold), Os^{3+} (10-fold), Re^{5+} (7.5-fold), V^{4+} (7-fold), and Rh^{3+} (5-fold) in terms of the chloroform oxidation. On the other hand, Co^{3+}- and Al^{3+}-doped TiO_2 exhibited reduced photoreactivities. The data presented in Figure 2 are plotted in Figure 3 to show a direct linear correlation between Φ_{CHCl_3} and Φ_{CCl_4/Cl^-}.

The observed photodegradation rates for $CHCl_3$ (ν_{ox}) were found to depend on the incident light intensity for both the undoped and Fe^{3+}-doped (0.5%) Q-sized TiO_2 (Figure 4). In the case of undoped Q-sized TiO_2 $\nu_{ox} \propto I^{0.77}$ while for Fe^{3+}-

TABLE 1: Summary of the Chloroform Degradation Quantum Yields (Φ_{CHCl_3}, %) for Several Doped TiO_2 Colloids at Various Dopant Concentrations, $[CHCl_3]_0$ = 3.15 mM

	dopant concentration (at. %)									
dopant	0.0	0.1	0.25	0.5	1.0	2.0	3.0	5.0	pH	light intensity (einstein L^{-1} min^{-1})
Fe^{3+}	0.08	0.78		1.19	0.80	0.51		0.10	2.7 ± 0.1	0.75×10^{-4}
V^{4+}	0.08	0.38		0.49	0.35	0.22	0.08			
V^{3+}	0.08	0.31	0.40	0.53	0.36	0.19	0.15			
Re^{5+}	0.08	0.27	0.31	0.41	0.32	0.24	0.10			
Mo^{5+}	0.08	0.49	0.32	0.31	0.30	0.20	0.12			
Ru^{3+}	0.08	0.09	0.31	0.38	0.37	0.18	0.15			
Mn^{3+}	0.16	0.20	0.32	0.59	0.57	0.23	0.10		11.1 ± 0.3	1.28×10^{-4}
Co^{3+}	0.16	0.18	0.10	0.08	0.04	<0.03	<0.03			
Rh^{3+}	0.16	0.48	0.61	0.87	0.46	0.18	0.04			

Li^{+} 0.15 <0.08 (0.90)											
	Mg^{2+} 0.14 <0.08 (0.86)	V^{3+} 1.02 1.72 (0.78)	V^{5+} 0.51 0.66 (0.68)						Al^{3+} 0.08 <0.08 (0.68)		
Ti^{4+*} 0.16 <0.08 (0.75)	V^{4+} 1.09 1.60 (0.72)	Cr^{3+} 0.21 0.16 (0.76)	Mn^{3+} 0.59 0.12 (0.79)	Fe^{3+} 2.38 1.74 (0.79)	Co^{3+} 0.08 <0.08 (0.69)	Ni^{2+} 0.50 0.09 (0.83)		Zn^{2+} 0.20 <0.08 (0.88)	Ga^{3+} 0.15 <0.08 (0.76)		
Zr^{4+} 0.09 0.11 (0.86)	Nb^{5+} 0.23 <0.08 (0.78)	Mo^{5+} 1.82 1.59 (0.75)		Ru^{3+} 1.72 0.38 (0.82)	Rh^{3+} 0.87 0.44 (0.81)					Sn^{4+} 0.11 <0.08 (0.83)	Sb^{5+} 0.15 <0.08 (0.74)
	Ta^{5+} 0.27 <0.08 (0.78)		Re^{5+} 1.20 0.80 (0.72)	Os^{3+} 1.60 0.84							

Figure 2. Periodic chart of the photocatalytic effects of various metal ion dopants in TiO_2. The upper boldfaced numbers are the quantum yields (%) for the oxidative chloroform degradation, Φ_{CHCl_3}, and the lower numbers are the quantum yields (%) for Cl^- production from the reductive dechlorination of carbon tetrachloride, Φ_{CCl_4/Cl^-}. The numbers in the parentheses are the ionic radii (Å)[43] for a coordination number of 6. All the oxidation states represent those of the precursor metal ions. All dopant concentrations are 0.5 at.% except Mo^{5+} (0.1 at.%). Ti^{4+}* refers to the undoped TiO_2 (see Experimental Section for details).

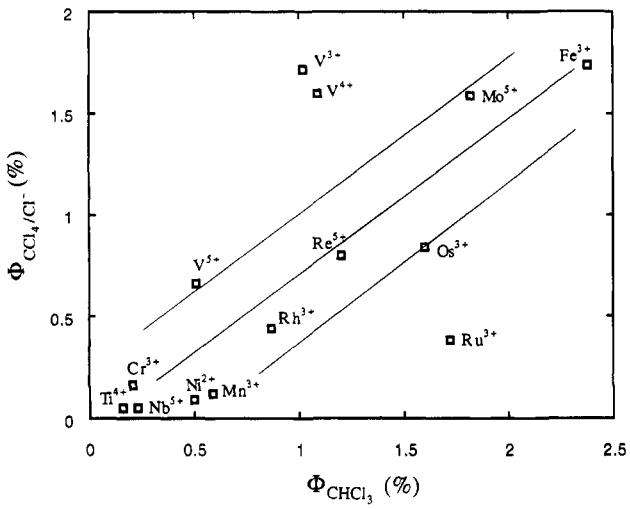

Figure 3. Correlation plot between the oxidation quantum yield (Φ_{CHCl_3}) and the reduction quantum yield (Φ_{CCl_4/Cl^-}) from the data of Figure 2. Some dopants, which show little effect on the photoreactivity, are omitted for clarity of the figure. The straight lines are drawn only as a visual guide.

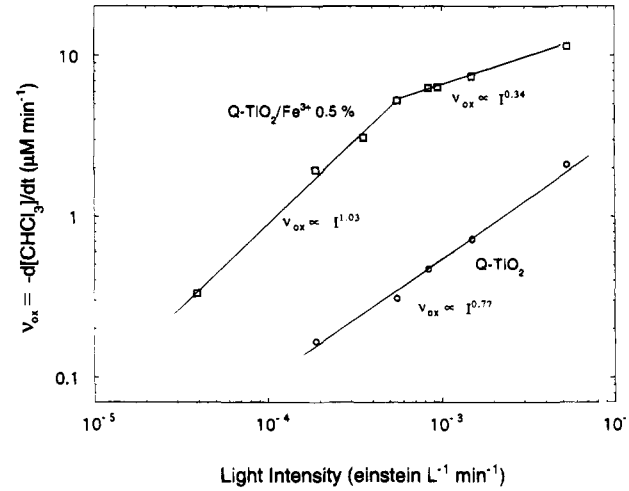

Figure 4. Light intensity (I) dependence of the photodegradation rate of chloroform (v_{ox}) for the undoped and Fe^{3+}-doped (0.5%) Q-sized TiO_2 under the condition of $[CHCl_3]_0$ = 3.15 mM and pH 11.

doped Q-sized TiO_2 two distinct regimes of $v_{ox} \propto I^{1.03}$ ($I_0 < 5.5 \times 10^{-4}$ einstein L^{-1} min^{-1}) and $v_{ox} \propto I^{0.34}$ ($I_0 > 5.5 \times 10^{-4}$ einstein L^{-1} min^{-1}) were observed. The photon flux into a single particle at $I_0 = 5.5 \times 10^{-4}$ einstein L^{-1} min^{-1} corresponds to a flux of ~1 photon/(particle s).

Since the steady-state photolyses (λ_{ex} = 320 nm) and the laser flash photolyses (λ_{ex} = 355 nm) were performed at different wavelengths, photoreactivities of undoped Q-sized TiO_2 and Fe^{3+}-doped (0.5%) Q-sized TiO_2 were measured at the two different wavelength regions in order to ensure that the photochemical processes were wavelength-independent. Two UV band-pass filters were used. One transmitts light in the range 300–340 nm (centered at 320 nm, $I = 1.39 \times 10^{-4}$ einstein L^{-1} min^{-1}), and the other transmits light in the range 310–400 nm (centered at 360 nm, $I = 1.89 \times 10^{-4}$ einstein L^{-1} min^{-1}). In both cases, the ratio of Φ_{CHCl_3}(Fe^{3+}-doped TiO_2) to Φ_{CHCl_3}(undoped TiO_2) was 12.

The photoreductive dechlorination of CCl_4 was investigated as a function of the hole scavenger (CH_3OH) concentration. In Figure 5, the ratios of the chloride production rates with methanol to those without methanol are plotted as a function of the added methanol concentration for the undoped and Fe^{3+}-doped (0.5%) Q-sized TiO_2. The relative rates for the undoped Q-sized TiO_2 are enhanced up to 13-fold with added methanol while the Fe^{3+}-doped Q-sized TiO_2 shows little change.

Photoreactivity Study of Heat-Treated Samples. Undoped and several doped Q-sized TiO_2 samples were heat-treated under temperatures of 100, 200, and 400 °C for 4 h each in order to investigate the effect of particle agglomeration and sintering on the photoreactivity. All suspensions of heat-treated TiO_2 samples were turbid due to the agglomeration. A 305 nm cutoff long-pass filter was used for irradiation instead of a 320 nm UV interference filter due to the low reactivity of the heated

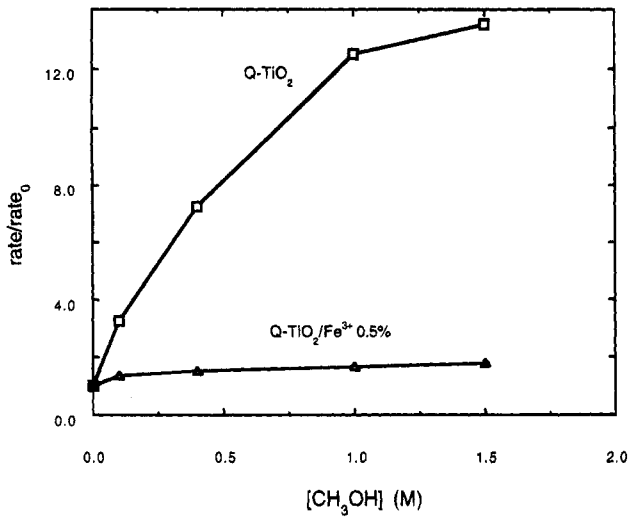

Figure 5. Ratio of relative chloride production from CCl_4 dechlorination as a function of added methanol concentration for the undoped and the Fe^{3+}-doped (0.5%) Q-sized TiO_2.

TABLE 2: Effects of Heat Treatment at Various Temperatures on the Photoreactivities of the Undoped and Doped TiO_2 Measured in Terms of the Chloroform Degradation Rate, v_{CHCl_3} (μM min^{-1}); Suspension Concentrations Are Given in Brackets

dopant	unheated [0.5 g/L] (pH 2.9−2.6)	100 °C/4 h [0.5 g/L] (pH 3.1−2.8)	200 °C/4 h [1 g/L] (pH 3.6−3.3)	400 °C/4 h [1 g/L] (pH 5.5−4.6)
undoped	1.5	1.4	1.5	0.1
Fe^{3+} (0.5%)	12.5	7.2	0.7	0.03
V^{4+} (0.5%)	8.2	4.6	0.4	0.1
Mo^{5+} (0.1%)	7.5	6.1	1.1	0.07
Ru^{3+} (0.5%)	4.6	1.0	0.6	0.07
Rh^{3+} (0.5%)	2.2	1.2	0.2	0.00

samples. Table 2 summarizes the photoreactivities of heat-treated undoped and doped samples. All the doped TiO_2 samples lose their photoreactivity gradually as the sintering temperature is increased. Doped TiO_2 samples heated above 200 °C show lower reactivities than the undoped TiO_2. The particle size data obtained from TEM and SEM analysis of the heat-treated samples show that both the primary particle size (up to ~40 nm) and the aggregate size (up to ~5 μm) of the particles increase as the heating temperature increases up to 400 °C. Figure 6 shows the TEM pictures of Q-sized TiO_2 (unheated) particles and an agglomerated TiO_2 (400 °C/4 h) particle which consists of fused nanocrystals of doped (Fe^{3+}, 0.5%) TiO_2. The loss of photoactivity of doped heat-treated samples cannot be ascribed to a simple decrease in reactive surface area due to agglomeration because the photoreactivity of the undoped sample remains constant up to 200 °C.

Transient Absorption Spectra of Doped Q-Sized TiO_2. The transient absorption decays of the undoped Q-sized TiO_2 were monitored over the wavelength range 450−750 nm. The absorption spectrum showed a broad characteristic peak attributed to trapped electrons with $\lambda_{max} \approx 600$ nm.[31] The decay kinetics were found to be independent of λ. The transient absorption decays monitored at 600 nm for several doped Q-sized TiO_2 are shown in Figures 7−9. In Figure 7, the transient absorption decays of Fe^{3+}-, Co^{3+}-, V^{4+}-, and Al^{3+}-doped (all at 0.5%) TiO_2 are compared to an undoped sample in microsecond time region. The transient decays of Mo^{5+}-(0.1%)- and Ru^{3+}(0.5%)-doped TiO_2 were similar to that of V^{4+}-doped sample over the same time scale. The absorption signals were developed within the laser pulse duration and decay rapidly until a plateau was reached. Further decay occurred on a longer time scale. In general, doped Q-sized TiO_2 samples that were shown to increase (or decrease) photoreactivity have higher (or lower) absorption signal intensities than the others in the plateau region. The average number of e^-/h^+ pairs present initially in one undoped TiO_2 particle (Figure 7a) is 0.66 based on an extinction coefficient of 1200 M^{-1} cm^{-1} for the electron absorption at 600 nm.[31] This corresponds roughly to 10% of the absorbed photons. All excited-state decays in the microsecond time region were fitted to the following double-exponential equation:

$$A(t) = A_\infty + C_1 \exp(-k_1 t) + C_2 \exp(-k_2 t) \qquad (5)$$

In Table 3, the fitting parameters for the doped TiO_2 samples are listed along with their corresponding quantum yields, Φ_{CHCl_3} and Φ_{CCl_4/Cl^-}. No correlation was seen between the photoreactivity and either of the decay constants (k_1 and k_2). However, the A_∞, which is determined from the plateau region, appears to correlate well with the photoreactivity. Figure 10 shows a linear correlation between A_∞ and Φ (oxidation, reduction, and their average). The correlation is best represented by the plot of Φ_{avg} vs A_∞. A_∞ represents the residual absorption by the trapped charge carriers that survive recombination over the nano- to microsecond time domain. This trend is clearly shown in Figure 8, in which the absorption decays are followed over the millisecond time scale. The absorption signals of Fe^{3+}-, V^{4+}-, and Ru^{3+}-doped TiO_2 show much longer characteristic decay times that extend out to 50 ms while, in contrast, the undoped sample shows a complete decay within 200 μs. These results are consistent with the results obtained by Grätzel and co-workers[7b] for Fe^{3+}-doped TiO_2. The Ru^{3+}-doped TiO_2 shows very slow decay in this time scale compared to the others. Figure 9 shows the absorption decays of Fe^{3+}-doped sample at three different dopant concentrations (0.1, 0.5, and 3.0%). As is shown in Table 1, most of the tested dopants have an optimal concentration of 0.5 at.% for enhanced photoreactivity. The observed enhancements are consistent with the transient absorption measurements. The A_∞ shows a maximum at 0.5% dopant concentration in both millisecond and microsecond regions, while it is reduced at both lower and higher dopant concentrations.

Discussion

Energetics of Charge Trapping/Detrapping and Photoreactivity in Doped TiO_2. Metal ion dopants influence the photoreactivity of TiO_2 by acting as electron (or hole) traps and by altering the e^-/h^+ pair recombination rate through the following process:[7,8b,14,15]

$$M^{n+} + e_{cb}^- \rightarrow M^{(n-1)+} \quad \text{electron trap}$$

$$M^{n+} + h_{vb}^+ \rightarrow M^{(n+1)+} \quad \text{hole trap}$$

where the energy level for $M^{n+}/M^{(n-1)+}$ lies below the conduction band edge (E_{cb}) and the energy level for $M^{n+}/M^{(n+1)+}$ above the valence band edge (E_{vb}). Available energy levels of metal ion impurities in rutile TiO_2[32,33] are shown in Figure 11. Introduction of such energy levels in the band gap induces the red shift in the band gap transition and the visible light absorption (Figure 1) through a charge transfer between a dopant and CB (or VB) or a d−d transition in the crystal field. The band gap shift of 0.12 eV in Fe^{3+}-doped (2%) TiO_2 can be assigned to the charge-transfer transition from the d orbital of Fe^{3+} to CB according to the energy level diagram in Figure 11. The tailing of the absorption band into the visible region for

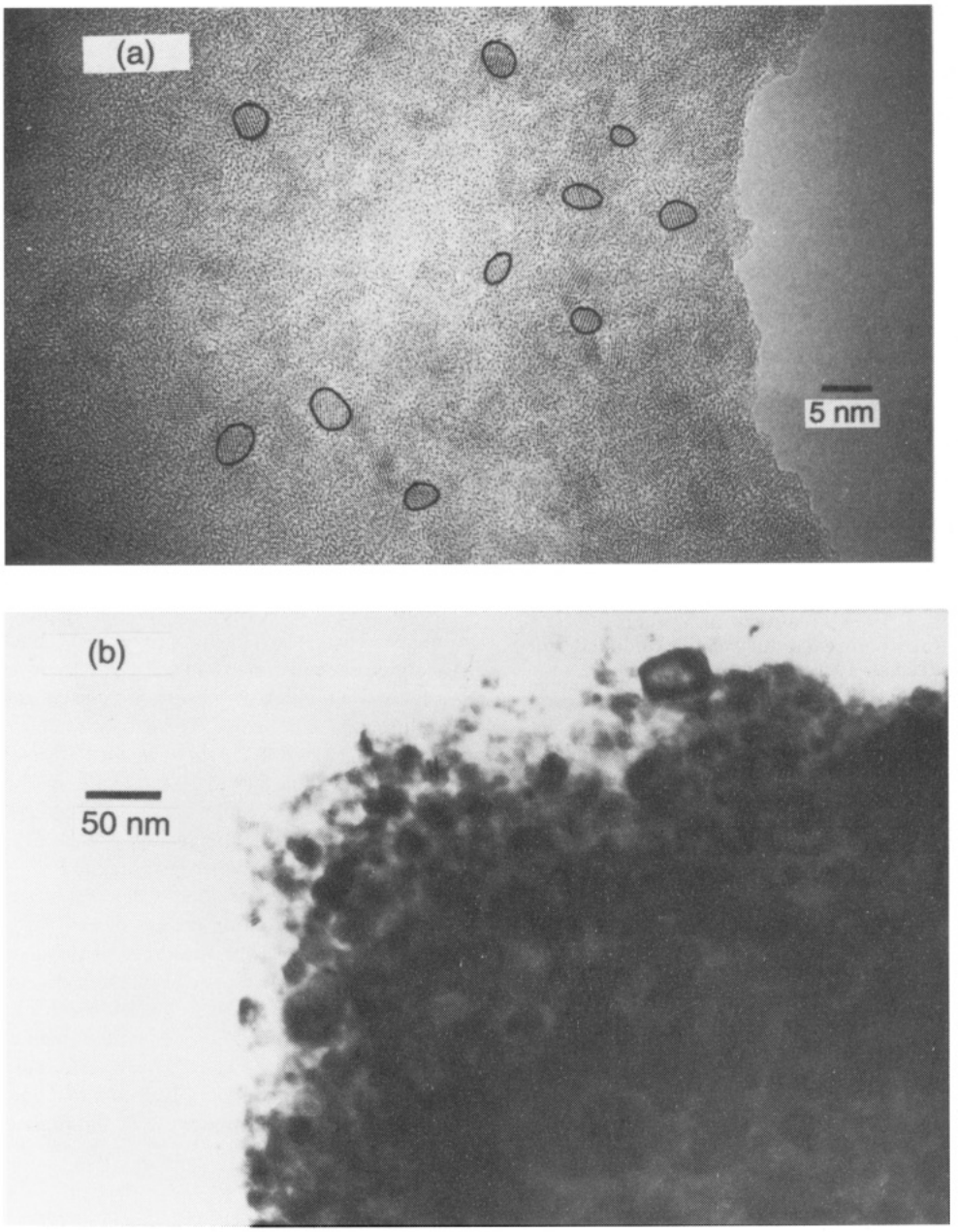

Figure 6. TEM pictures of (a) Q-sized TiO_2 particles and (b) an aggregate of small particles (Fe^{3+}, 0.5%) resulting from heating at 400 °C/4 h. Several Q-sized particles are outlined for clarity.

V^{4+}- and Mn^{3+}-doped TiO_2 (Figure 1c) can be also assigned to a similar charge-transfer band. The separate absorption band centered at 437 nm (2.8 eV) of Ru^{3+}-doped TiO_2 can be assigned to the donor transition of Ru^{3+} into CB:[33]

$$Ru^{3+} \rightarrow Ru^{4+} + e_{cb}^- \quad (6)$$

From the onset (520 nm) of this band we suggest the redox level of Ru^{3+}/Ru^{4+} in anatase Q-sized TiO_2 is located 2.4 eV below E_{cb}, which might be slightly different from the redox level in the bulk anatase. The Ru^{2+}/Ru^{3+} redox level in Figure 11 suggests a possible acceptor transition in rutile:

$$Ru^{3+} \rightarrow Ru^{2+} + h_{vb}^+ \quad (7)$$

This transition is suggestive from the absorption around 360–380 nm in Figure 1b which can not be accounted for by an overlap of the band gap transition and the 437 nm band. The absence of photoactivity of Ru^{3+}-doped colloid with $\lambda > 390$ nm indicates the ineffectiveness of the sole electron excitation (eq 4) for the interfacial charge transfer. Herrmann et al.[13c] also reported that the photoconductance spectrum of Cr^{3+}-doped TiO_2 did not parallel the absorption curve in the visible region.

According to the energy level diagram of Figure 11, V^{4+}, Mn^{3+}, Co^{3+}, and Ru^{3+} can act as both hole and electron traps, while Fe^{3+}, Cr^{3+}, and Ni^{2+} can serve only as hole traps. We note that the energy levels in the Q-sized anatase ($E_g = 3.37$ eV) may not be identical with those of the single-crystal rutile ($E_g = 3.0$ eV). For example, it has been suggested that Fe^{3+} can be an electron trap as well in anatase.[8b] In order to continue our analysis, we will assume that the energy levels in Figure 11 are applicable to Q-sized TiO_2. The apparent energy levels, however, do not seem to provide a unifying explanation that is consistent with our observations.

Even though Fe^{3+} and Cr^{3+} have similar energy levels in the TiO_2 lattice (0.1–0.3 eV above E_{vb}), similar ionic radii (0.79 vs 0.76 Å), and identical oxidation states, their efficiencies as dopants with respect to photoreactivity are substantially different.

Differences in photoactivity of Fe^{3+}- and Cr^{3+}-doped TiO_2 electrodes have been ascribed to differences in the diffusion lengths of the minority carriers (2 μm for Fe^{3+} vs 0.2 μm for Cr^{3+}).[20a] However, this explanation is not appropriate to very small particles whose dimension is much smaller than the characteristic diffusion length. Moser et al.[7b] attributed the inhibition of e^-/h^+ recombination in Fe^{3+}-doped TiO_2 colloids to the local separation of trapped charge carriers. Even though it is widely accepted that the photoreactivities of doped TiO_2 are related to the dopant trap site, it is often neglected that the trapped charges should be transferred to the interface to initiate the photoreactions. In this context, the energetics of the charge release and migration in the lattice is equally important as well as the charge-trapping energetics. A general photochemical charge-trapping, recombination, detrapping, and migration mechanism in the presence of metal ion dopants can be proposed as follows:

charge pair generation

$$TiO_2 + h\nu \rightarrow e_{cb}^- + h_{vb}^+ \quad (8)$$

$$M^{n+} + h\nu \rightarrow M^{(n+1)+} + e_{cb}^- \quad (9)$$

$$M^{n+} + h\nu \rightarrow M^{(n-1)+} + h_{vb}^+ \quad (10)$$

charge trapping

$$Ti^{4+} + e_{cb}^- \rightarrow Ti^{3+} \quad (11)$$

$$M^{n+} + e_{cb}^- \rightarrow M^{(n-1)+} \quad (12)$$

$$M^{n+} + h_{vb}^+ \rightarrow M^{(n+1)+} \quad (13)$$

$$>OH^- + h_{vb}^+ \rightarrow >OH^\bullet \quad (14)$$

charge release and migration

$$M^{(n-1)+} + Ti^{4+} \rightarrow M^{n+} + Ti^{3+} \quad (15)$$

$$M^{(n+1)+} + >OH^- \rightarrow M^{n+} + >OH^\bullet \quad (16)$$

recombination

$$e_{cb}^- + h_{vb}^+ \rightarrow TiO_2 \quad (17)$$

$$Ti^{3+} + >OH^\bullet \rightarrow Ti^{4+} + >OH^- \quad (18)$$

$$M^{(n-1)+} + h_{vb}^+ \rightarrow M^{n+} \quad (19)$$

$$M^{(n-1)+} + >OH^\bullet \rightarrow M^{n+} \quad (20)$$

$$M^{(n+1)+} + e_{cb}^- \rightarrow M^{n+} \quad (21)$$

$$M^{(n+1)+} + Ti^{3+} \rightarrow M^{n+} \quad (22)$$

interfacial charge transfer

$$e_{cb}^- \text{ (or } Ti^{3+}, M^{(n-1)+}) + O \rightarrow O^- \quad (23)$$

$$h_{vb}^+ \text{ (or } >OH^\bullet, M^{(n+1)+}) + R \rightarrow R^+ \quad (24)$$

where M^{n+} is a metal ion dopant, O is an electron acceptor (oxidant), and R is an electron donor (reductant). The origin of the different photoreactivities between Fe^{3+} and Cr^{3+} can be explained based on the above mechanism and the energy level diagram in Figure 11.

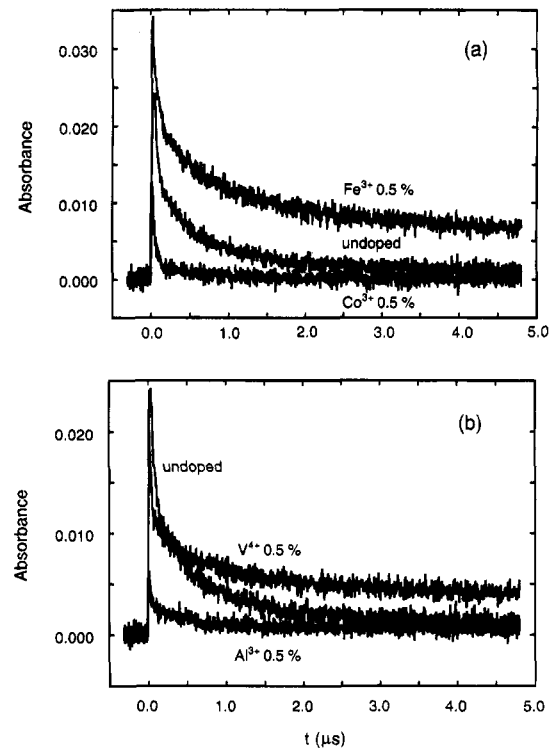

Figure 7. Transient absorption decays observed at 600 nm in the microsecond time scale for (a) undoped, Fe^{3+} (0.5%) and Co^{3+} (0.5%) and (b) undoped, V^{4+} (0.5%) and Al^{3+} (0.5%) doped Q-sized colloids.

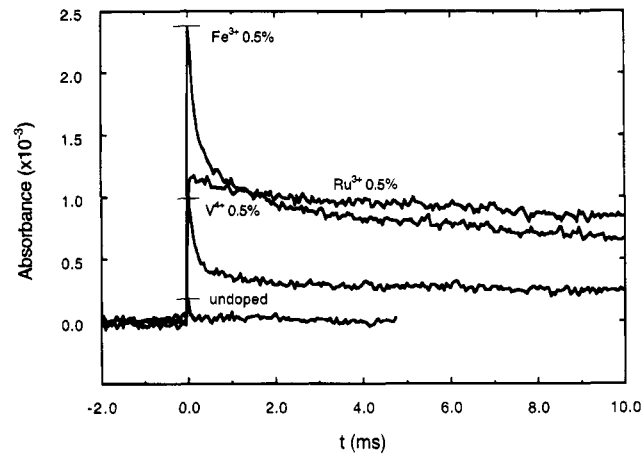

Figure 8. Transient absorption decays observed at 600 nm in the millisecond time scale for Fe^{3+} (0.5%), V^{4+} (0.5%), Ru^{3+} (0.5%) doped and undoped Q-sized colloids.

The hole trapping by both Fe^{3+} and Cr^{3+} (eq 13) after the photoexcitation is equally favorable while the electron trapping is probable only for Fe^{3+} (eq 12). The trapped holes in Fe^{4+} and Cr^{4+} either migrate to the surface (eq 16) or recombine (eqs 21 and 22). Photoexcited electron in the presence of Cr^{3+}, which cannot trap an electron, quickly recombines with a trapped hole (eq 21). The trapped hole embodied in Fe^{4+} has longer lifetime due to the immobilized electron in Fe^{2+}. According to crystal field theory, Fe^{2+} is relatively unstable due to the loss of exchange energy on going from d^5 (half-filled high spin) to d^6 and tends to return to $Fe^{3+}(d^5)$. However, the Fe^{2+}/Fe^{3+} energy level lies close to Ti^{3+}/Ti^{4+} level. As a consequence of this proximity, the trapped electron in Fe^{2+} can be easily

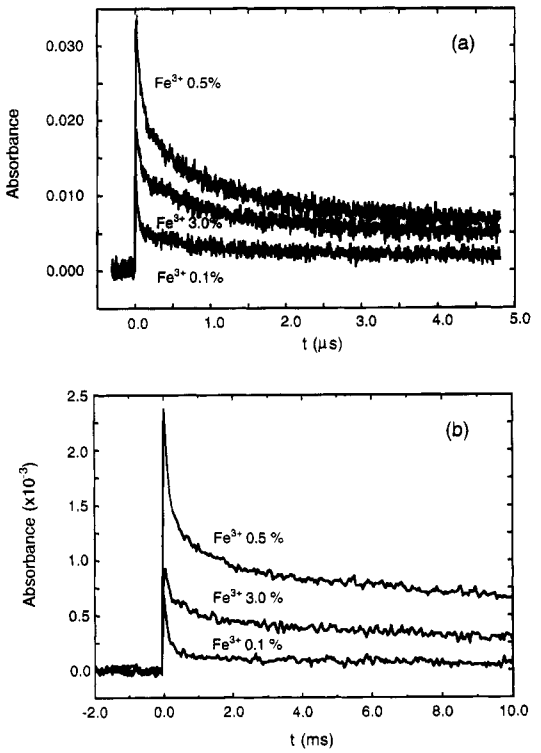

Figure 9. Transient absorption decays observed at 600 nm for Fe^{3+}-doped colloids at 0.1, 0.5, and 3.0% Fe^{3+} concentration in the (a) microsecond time scale and (b) millisecond time scale.

TABLE 3: Comparison of the Fitting Parameters (Eq 5) from the Transient Absorption Decays with the Photocatalytic Quantum Yields (%) from Figure 2 for Various Doped Q-Sized TiO_2

dopant	A_∞ ($\times 10^{-3}$)	k_1 ($\times 10^7$)	k_2 ($\times 10^6$)	Φ_{ox}	Φ_{red}	Φ_{avg}
undoped	1.31	1.79	1.36	0.16	0.08	0.12
Fe^{3+}	6.69	1.23	0.84	2.38	1.74	2.06
V^{4+}	4.22	3.02	0.98	1.09	1.60	1.35
Mo^{5+}	3.62	2.18	0.99	1.82	1.59	1.71
Ru^{3+}	3.45	6.98	1.67	1.72	0.38	1.05
Rh^{3+}	1.99	0.86	0.60	0.87	0.44	0.66
Mn^{3+}	1.04	2.74	1.47	0.59	0.12	0.34
Nb^{5+}	0.95	3.82	1.25	0.23	0.08	0.16
Al^{3+}	0.60	4.16	1.60	0.08	0.08	0.08
Cr^{3+}	0.55	3.19	1.26	0.21	0.16	0.19
Co^{3+}	0.04	2.56	1.35	0.08	0.08	0.08

transferred to a neighboring surficial Ti^{4+} (eq 15), which then leads to interfacial electron transfer (eq 23).

The effect of the energy levels of the dopants on photoreactivity can be generalized based upon the above arguments. First of all, dopants should act as both electron traps and hole traps to be photoactive. Trapping either an electron or a hole alone is ineffective because the immobilized charge species quickly recombines with its mobile counterpart. ESR studies[7a,34] have shown that Mo^{6+} and Mo^{5+} coexisted in the TiO_2 lattice where they act an electron trap and a hole trap, respectively. This explanation is in accord with the high photoactivity of Mo^{5+} as a dopant. Judging from the fact that V^{3+} is readily oxidized to V^{4+} under ambient conditions,[35] the V^{3+} listed in Figure 2 may actually be present in the TiO_2 lattice as V^{4+}, which can act as both an electron trap and a hole trap. Thus, the photoreactivities of V^{3+} and V^{4+} are very similar. On the other hand, the photoactivity of V^{5+} is significantly lower than that of V^{4+} since V^{5+} can only trap electrons. Even though the energy levels of the other metal ions are not available, some general trends are apparent based on considerations of the electronic configuration of the dopants. All dopants with a

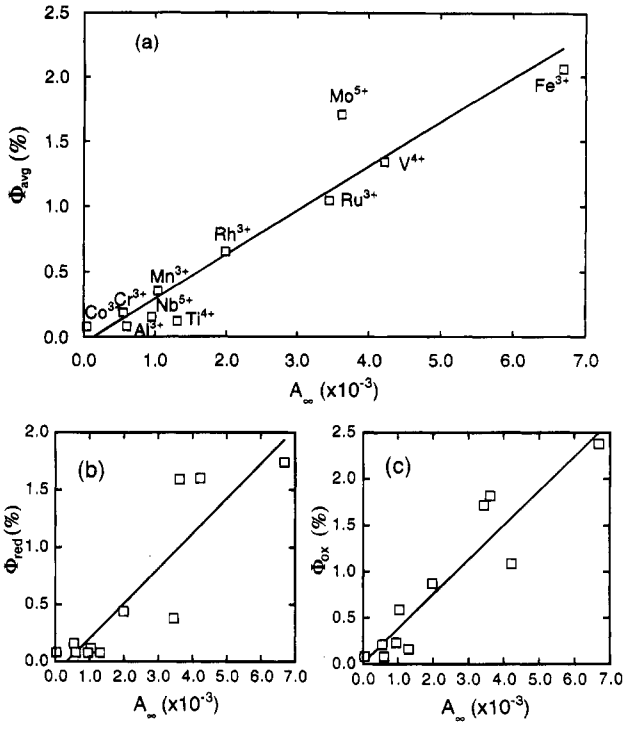

Figure 10. Correlation plot between the quantum yields [(a) Φ_{avg}, (b) Φ_{red}, and (c) Φ_{ox}] and A_∞ from Table 3.

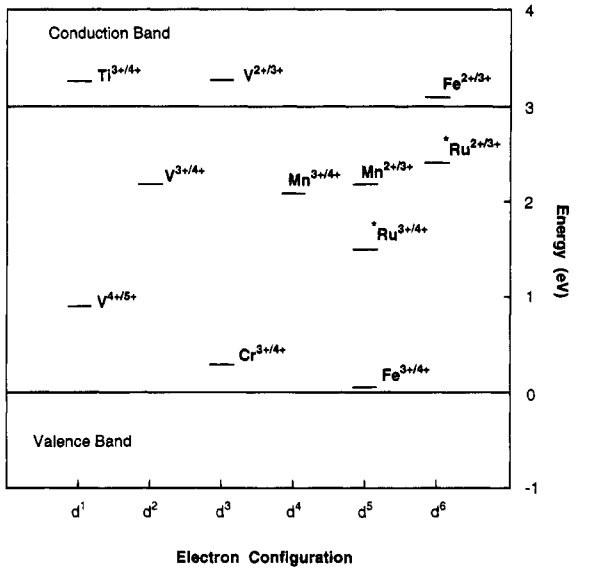

Figure 11. Energy levels of impurity ions in rutile proposed by Mizushima et al.[32] and Triggs (*).[33]

closed-shell electronic configuration (Li^+, Mg^{2+}, Al^{3+}, Zn^{2+}, Ga^{3+}, Zr^{4+}, Nb^{5+}, Sn^{4+}, Sb^{5+}, and Ta^{5+}) have little effect on the observed photoreactivity.

The stability of a closed electronic shell makes electron (or hole) trapping unfavorable. For example, low reactivity of Co^{3+}, which is known to have low-spin configuration (t_{2g}^6 in an octahedral field) in many oxides,[36] could be attributed to its stable partly closed electronic configuration. The significant deviation of V^{4+} and Ru^{3+} from the linear correlation in Figure 3 may arise, in part, from the stable closed-shell configuration of $V^{5+}(d^0)$, a trapped hole, and the partly filled low-spin configuration of $Ru^{2+}(t_{2g}^6)$, a trapped electron. However, this general requirement is not sufficient to predict a good dopant. For example, we did not observe an enhanced photoreactivity with Mn^{3+}, which can trap both electrons and holes.

The second prerequisite for an effective dopant may involve the possibility of charge detrapping and migration to the surface of previously trapped charges. The importance of trapped charge migration was discussed above for Fe^{3+}. The low photoreactivity of Mn^{3+}-doped TiO_2 can be attributed to the low driving force for electron detrapping from Mn^{2+} due to the small energy difference between Mn^{2+} and Mn^{3+}. We extend the caveat that all energetic considerations are valid only for dopants located close to the surface site at which the interfacial charge transfer occurs. Since the diameter of the exciton in Q-sized TiO_2 is approximately 20 Å, the prerequisites are met within a nanosecond of excitation.

Recombination, Trapping, Interfacial Transfer of Charge Carriers, and Photoreactivity in Doped TiO_2. We should keep in mind that Q-sized particles represent an unusual case with respect to electron transfer at the semiconductor–liquid interface compared to their bulk-phase counterparts. A distinctive feature of Q-sized semiconductors is the lack of appreciable band bending. The total potential drop within a Q-sized particle is given by the equation[37]

$$\Delta\phi = kT/6e(r_0/L_D)^2 \qquad (25)$$

where r_0 is the radius of the particle and L_D is the Debye length. For a particle of 3 nm diameter with 0.5 at.% of dopants, $\Delta\phi$ is calculated to be 0.01 V. Considering that the magnitude of the potential drop across the space-charge layer should not be less than 0.1 V for an efficient e^-/h^+ separation,[20e] the small potential drop for Q-sized TiO_2 (0.01 V) is an insufficient driving force for the charge pair separation within a particle. Moreover, for Q-sized particles the wave function of the charge carrier spreads over the entire semiconductor cluster.[38] As a result, both electrons and holes are readily available at the interface. Oxidation reactions by VB holes and reduction reactions by CB electrons can thus occur concurrently, thereby satisfying the condition of electroneutrality on a semiconductor particle in which an e^- reacts (eq 23) for each h^+ reacted (eq 24). The correlation between the oxidation and reduction quantum yields in Figure 3 can be explained by the near equal availability of electrons and holes on the surface of Q-sized particles. A direct correlation of oxidation and reduction efficiencies cannot be expected from a semiconductor electrode or large bulk-phase particles (approximately micrometers) in which the space-charge layer is developed near the surface and photogenerated e^-/h^+ pairs are locally separated. The apparent disagreement in the reported photoactivity between this work and previous investigations of the effects of dopants for electrodes[20] or bulk-phase particles[14–16] can be ascribed to the lack of band bending in Q-sized semiconductors.

The photoreactivities of doped TiO_2 widely vary depending upon the specific dopant as shown in Figure 2. The origin of these different photoreactivities appears to be related to the efficiencies of the dopants in trapping charge carriers and mediating interfacial charge transfer. This idea is supported by the transient absorption decays of the trapped electron as shown in Figures 7 and 8. The trapped electron in TiO_2 colloids gives rise to a broad absorption band (400–1000 nm) with a nominal maximum around 600 nm,[31] while the trapped hole exhibits a broad absorption (400–800 nm) band with $\lambda_{max} = 475$ nm.[22a] The overlap of absorption bands near 600 nm seems to be negligible over the nanosecond time frame because electron trapping is much faster ($\tau \sim 30$ ps) than the hole trapping ($\tau \sim 250$ ns).[39] However, this overlap may not be negligible over the microsecond time domain that we are probing. Hole trapping is able to compete effectively with recombination under conditions of our experiment where only 0.66 e^-/h^+ pair per particle is created by the laser pulse. Furthermore, the presence of metal ion dopants provides more trap sites for holes in addition to the surface trap sites ($>OH^-$).

$$e_{cb}^- \rightarrow e_{tr}^- \quad (\text{as } Ti^{3+} \text{ or } M^{(n-1)+}) \qquad \tau \sim 30 \text{ ps} \qquad (26a)$$

$$h_{vb}^+ \rightarrow h_{tr}^+ \quad (\text{as } >OH^\bullet \text{ or } M^{(n+1)+}) \qquad \tau \sim 250 \text{ ns} \qquad (26b)$$

$$e_{tr}^- + h_{vb}^+ \rightarrow TiO_2 \qquad \tau \sim 30 \text{ ns} \qquad (26c)$$

$$e_{tr}^- + h_{tr}^+ \rightarrow TiO_2 \qquad \text{slow} \qquad (26d)$$

Considering that the mean lifetime of a single electron–hole pair in a TiO_2 particle (12 nm diameter) was determined to be 30 ns (eq 26c),[39] the appearance of a plateau in the absorption decay curves (microsecond domain) of the doped TiO_2 colloids (Figure 7) indicates a slow recombination process described by eq 26d. Therefore, A_∞ in eq 5 should be regarded as the relative absorption by both e_{tr}^- and h_{tr}^+ even though their proportions are unknown. The trapped charge carriers have a sufficiently long lifetime to reach the surface by detrapping (eqs 15 and 16) and electron tunneling. As a consequence, the higher the A_∞ value, the higher the observed photoreactivity.

The role of a metal ion dopant as a direct mediator of the interfacial charge transfer is indicated by the data summarized in Table 2. Given the size of Q-sized particles the dopants are located within 10–20 Å from the surface. Under these conditions, all dopants can be considered as located in the surface region where the charge transfer to the interface is easily achieved. As the small Q-sized particles agglomerate upon heating, dopants are isolated far from the surface with a much lower chance of transferring trapped charge carriers to the interface. Thus, the data of Table 2 show steadily decreasing photoreactivities of doped TiO_2 with an increase in sintering temperature. As a result of particle agglomeration, the dopants are more likely to serve as recombination centers than as trap sites for eventual charge transfer at the interface.

The curves shown in Figure 5 can be also interpreted in terms of the integral role of the dopant in mediating interfacial charge transfer. In undoped TiO_2, the increasing concentration of a hole scavenger (e.g., CH_3OH) increases the efficiency of interfacial charge transfer (hence the photoreactivity) since effective hole scavenging diverts an increasing fraction of charge carriers toward interfacial transfer. However, in doped colloids, the dopant (i.e., Fe^{3+}) functions as an interfacial charge-transfer mediator in the absence of hole scavengers. Thus, in the case of Fe^{3+}-doped TiO_2 the relative effect of additional hole scavengers is substantially less.

Several investigations[24,40] have shown that photocatalytic degradation rates undergo a transition from first-order to half-order kinetics with respect to incident light intensity, I with increasing I_0. In this study, this predicted transition was not observed up to $I = 5.30 \times 10^{-3}$ einstein L^{-1} $min^{-1} \sim 7$ photons/(particle·s) with the undoped Q-sized colloid (Figure 4). However, in a similar study using larger particles (Degussa P25, 0.5 g/L) Martin et al.[41] reported a transition at 6.87×10^{-5} einstein L^{-1} min^{-1}, which corresponds approximately to 75 photons/(particle·s) assuming an average particle size of 30 nm. These results imply that the Q-sized particles do not reach a saturation e^-/h^+ pair concentration since the number of photons absorbed per particle is much smaller for Q-sized colloids than for their bulk-phase counterparts. On the other hand, a first-order to a fractional-order (0.34) transition is seen for the Fe^{3+}-doped Q-sized TiO_2. The higher value of $d\nu_{CHCl_3}/dI$ in the doped colloids compared to the undoped colloids (1.03 vs 0.77) at

lower light intensities (<~1 photon/(particle s)) suggests that the trap sites provided by the dopants are more effectively transferring charge carriers than the intrinsic trap sites (e.g., Ti^{3+}). Above the transitional light intensity (>~1 photon/(particle s)), $d\nu_{CHCl_3}/dI$ decreases to 0.34, which suggests that recombination dominates over charge transfer. The fact that such a transition occurs at the light flux of ~1 photon/(particle s) implys that the charge transfer of trapped charge carriers to redox couples at the interface is a very slow process which might be extended up to a second. The slow transient absorption decays observed over the millisecond time frame region (Figure 8) may reflect the nature of this slow interfacial charge transfer. The observed low efficiencies at higher light intensities indicate that the dopants are efficient recombination centers (eqs 19–22) as well as good trapping sites. Thus, we conclude that the metal ion dopants are acting as effective trapping sites under low light intensities (i.e., with not all the dopant sites populated as traps). However, when the available trapping sites are fully occupied under conditions of high light intensities, the metal ion dopants become efficient recombination centers.

Dopant Concentration and Photoreactivity. For all of the dopants tested in Table 1, there appears to be an optimal dopant concentration above which the observed photoreactivity decreases. Even though similar results[6,8,10b,16] obtained for bulk-phase materials were interpreted in terms of a change in the space-charge layer thickness, the present results with Q-sized particles represent a different situation. In order to interpret these results, we note that recombination through tunneling between the trapped charge carriers (eq 26d) depends on the distance R separating the e^-/h^+ pair according to[37]

$$k_{recomb} \propto \exp(-2R/a_0) \quad (27)$$

where a_0 is the radius of the hydrogenic wave function of the trapped carriers. As a consequence, the recombination rate increases exponentially with the dopant concentration because the average distance between trap sites decreases with increasing the number of dopants confined within a particle. Considering that the solubility limit of iron in anatase is about 1 at%,[42] some surface enrichment of iron should be present at higher dopant concentrations. Such a heterogeneity should decrease photoreactivity as well. At lower concentrations below the optimal value, photoreactivity increases with an increasing dopant concentration because there are fewer trapping sites available. For example, in a 4 nm diameter particle there is only 1 dopant ion per particle at 0.1%, 5 at 0.5%, and 30 at 3.0%. Therefore, the appearance of an optimal dopant concentration in Q-sized TiO_2 can be explained by the balance of an increase in trapping sites leading to efficient trapping and fewer trapped carriers leading to longer lifetimes for interfacial charge transfer. This general argument is supported by the transient absorption decays of Figure 9. The absorption intensity is maximized at 0.5 at.% Fe^{3+} while it is reduced at both 0.1% and 3.0%. This means that the number of trapped carriers in a particle is the highest in 0.5% Fe^{3+}/TiO_2 for which the highest photoreactivity was observed.

Conclusions

Quantum yields for the steady-state photolyses of $CHCl_3$ and CCl_4 on doped Q-sized TiO_2 colloids are quantitatively correlated with the transient recombination dynamics of charge carriers. Photoreactivities are shown to increase with the concentration of trapped charge carriers that remain after an initial fast recombination between free charge carriers. The relative efficiency of a metal ion dopant depends on whether it serves as a mediator of interfacial charge transfer or as a recombination center. The ability of a dopant to function as an effective trap is related to the dopant concentration, the energy level of dopants within the TiO_2 lattice, their d electronic configuration, the distribution of dopants within the particles, the electron donor concentration, and the incident light intensity. Enhanced interfacial charge transfer in the presence of effective dopants appears to be the most important factor in enhancement of photoreactivity of doped TiO_2.

Acknowledgment. We are grateful to ARPA and ONR {N0014-92-J-1901} for financial support. We thank the Beckman Institute of Caltech for allowing us to use its laser resource center. Dean Willberg, Jay Winkler, Scot Martin, and Nicole Peill were critical to the success of this project.

References and Notes

(1) (a) Serpone, N., Pelizzetti, E., Eds. *Photocatalysis—Fundamentals and Applications*; Wiley Interscience: New York, 1989. (b) Fox, M. A.; Dulay, M. T. *Chem. Rev.* **1993**, *93*, 341.

(2) Ollis, D. F., Al-Ekabi, H., Eds. *Photocatalytic Purification and Treatment of Water and Air*; Elsevier: Amsterdam, 1993.

(3) (a) Vrachnou, E.; Grätzel, M.; McEvoy, A. J. *J. Electroanal. Chem.* **1989**, *258*, 193. (b) Moser, J.; Punchihewa, S.; Infelta, P. P.; Grätzel, M. *Langmuir* **1991**, *7*, 3012.

(4) Hong, A. P.; Bahnemann, D. W.; Hoffmann, M. R. *J. Phys. Chem.* **1987**, *91*, 2109.

(5) (a) Bahnemann, D. W.; Mönig, J.; Chapmann, R. *J. Phys. Chem.* **1987**, *91*, 3782. (b) Disdier, J.; Herrmann, J.-M.; Pichat, P. *J. Chem. Soc., Faraday Trans. 1* **1983**, *79*, 651.

(6) Navio, J. A.; Marchena, F. J.; Roncel, M.; Del la Rosa, M. A. *J. Photochem. Photobiol. A: Chem.* **1991**, *55*, 319.

(7) (a) Grätzel, M.; Howe, R. F. *J. Phys. Chem.* **1990**, *94*, 2566. (b) Moser, J.; Grätzel, M.; Gallay, R. *Helv. Chim. Acta* **1987**, *70*, 1596.

(8) (a) Schrauzer, G. N.; Guth, T. D. *J. Am. Chem. Soc.* **1977**, *99*, 7189. (b) Soria, J.; Conesa, J. C.; Augugliaro, V.; Palmisano, L.; Schiavello, M.; Sclafani, A. *J. Phys. Chem.* **1991**, *95*, 274.

(9) Bickley, R. I.; Lees, J. S.; Tilley, R. J. D.; Palmisano, L.; Schiavello, M. *J. Chem. Soc., Faraday Trans.* **1992**, *88*, 377.

(10) (a) Sclafani, A.; Palmisano, L.; Schiavello, M. *Res. Chem. Intermed.* **1992**, *18*, 211. (b) Palmisano, L.; Augugliaro, V.; Sclafani, A.; Schiavello, M. *J. Phys. Chem.* **1988**, *92*, 6710.

(11) (a) Kiwi, J.; Grätzel, M. *J. Phys. Chem.* **1986**, *90*, 637. (b) Ileperuma, O. A.; Tennakone, K.; Dissanayake, W. D. D. P. *Appl. Catal.* **1990**, *62*, L1.

(12) Kiwi, J.; Morrison, C. *J. Phys. Chem.* **1984**, *88*, 6146.

(13) (a) Highfield, J. G.; Pichat, P. *New. J. Chem.* **1989**, *13*, 61. (b) Wong, W. K.; Malati, M. A. *Sol. Energy* **1986**, *36*, 163. (c) Herrmann, J.-M.; Disdier, J.; Pichat, P. *Chem. Phys. Lett.* **1984**, *108*, 618.

(14) Luo, Z.; Gao, Q.-H. *J. Photochem. Photobiol. A: Chem.* **1992**, *63*, 367.

(15) Mu, W.; Herrmann, J.-M.; Pichat, P. *Catal. Lett.* **1989**, *3*, 73.

(16) Karakitsou, K. E.; Verykios, X. E. *J. Phys. Chem.* **1993**, *97*, 1184.

(17) (a) Sabate, J.; Anderson, M. A.; Kikkawa, H.; Xu, Q.; Cervera-March, S.; Hill, C. G., Jr. *J. Catal.* **1992**, *134*, 36. (b) Kikkawa, H.; O'Regan, B.; Anderson, M. A. *J. Electroanal. Chem.* **1991**, *309*, 91.

(18) Borgarello, E.; Kiwi, J.; Grätzel, M.; Pelizzetti, E.; Visca, M. *J. Am. Chem. Soc.* **1982**, *104*, 2996.

(19) Kutty, T. R. N.; Avudaithai, M. *Chem. Phys. Lett.* **1989**, *163*, 93.

(20) (a) Maruska, H. P.; Ghosh, A. K. *Sol. Energy Mater.* **1979**, *1*, 237. (b) Ghosh, A. K.; Maruska, H. P. *J. Electrochem. Soc.: Electrochem. Sci. Technol.* **1977**, *124*, 1516. (c) Salvador, P. *Sol. Energy Mater.* **1980**, *2*, 413. (d) Matsumoto, Y.; Kurimoto, J.; Amagasaki, Y.; Sato, E. *J. Electrochem. Soc.: Electrochem. Sci. Technol.* **1980**, *127*, 2148. (e) Gautron, J.; Lemasson, P.; Marucco, J.-F. *Faraday Discuss. Chem. Soc.* **1981**, *70*, 81.

(21) Choi, W.; Termin, A.; Hoffmann, M. R. *Angew. Chem., Int. Ed. Engl.* **1994**, *33*, 1091.

(22) (a) Bahnemann, D.; Henglein, A.; Lilie, J.; Spanhel, L. *J. Phys. Chem.* **1984**, *88*, 709. (b) Kormann, C.; Bahnemann, D. W.; Hoffmann, M. R. *J. Phys. Chem.* **1988**, *92*, 5196.

(23) Zepp, R. G.; Hoigne, J.; Bader, H. *Environ. Sci. Technol.* **1987**, *21*, 443.

(24) (a) Kormann, C.; Bahnemann, D. W.; Hoffmann, M. R. *Environ. Sci. Technol.* **1991**, *25*, 494. (b) The overall reaction stoichiometry is $CHCl_3 + H_2O + {}^1/_2O_2 \rightarrow CO_2 + 3HCl$.

(25) (a) Bard, A. J., Lund, H. Eds. *Encyclopedia of Electrochemistry of the Elements—Organic Section Vol. XIV*; M. Dekker: New York, 1973; p 34. (b) Mönig, J.; Bahnemann, D.; Asmus, K.-D. *Chem.-Biol. Interact.* **1983**, *47*, 15.

(26) Lillie, V. J.; Beck, G.; Henglein, A. *Ber. Bunsen-Ges. Phys. Chem.* **1971**, *75*, 458.

(27) Ross, A. B.; Neta, P. *Rate Constants for Reactions of Aliphatic Carbon-Centered Radicals in Aqueous Solution*, NSRDS-NBS 70; National Bureau of Standards: Washington, DC, 1982.

(28) Choi, W.; Hoffmann, M. R. Submitted to *Environ. Sci. Technol.*

(29) Heller, H. G.; Langan, J. R. *J. Chem. Soc., Perkin Trans.* **1981**, *2*, 341.

(30) Stowell, M. H. B.; Larsen, R. W.; Winkler, J. R.; Rees, D. C.; Chan, S. I. *J. Phys. Chem.* **1993**, *97*, 3054.

(31) Kölle, U.; Moser, J.; Grätzel, M. *Inorg. Chem.* **1985**, *24*, 2253.

(32) (a) Mizushima, K.; Tanaka, M.; Iida S. *J. Phys. Soc. Jpn.* **1972**, *32*, 1519. (b) Mizushima, K.; Tanaka, M.; Asai, A.; Iida, S.; Goodenough, J. B. *J. Phys. Chem. Solids* **1979**, *40*, 1129.

(33) Triggs, P. *Helv. Phys. Acta* **1985**, *58*, 657.

(34) Meriaudeau, P. *Chem. Phys. Lett.* **1980**, *72*, 551.

(35) Bielanski, A.; Dyrek, K.; Serwicka, E. *J. Catal.* **1980**, *66*, 316.

(36) Cox, P. A. *Transition Metal Oxides: An Introduction to their Electronic Structure and Properties*; Clarendon Press: Oxford, 1992; p 121.

(37) Grätzel, M. *Heterogeneous Photochemical Electron Transfer Reactions*; CRC Press: Boca Raton, FL, 1987.

(38) Brus, L. *J. Phys. Chem.* **1986**, *90*, 2555.

(39) Rothenberger, G.; Moser, J.; Grätzel, M.; Serpone, N.; Sharma, D. K. *J. Am. Chem. Soc.* **1985**, *107*, 8054.

(40) (a) Okamoto, K.; Yamamoto, Y.; Tanaka, H.; Itaya, A. *Bull. Chem. Soc. Jpn.* **1985**, *58*, 2023. (b) Turchi, C. S.; Ollis, D. F. *J. Catal.* **1990**, *122*, 178.

(41) Martin, S. T.; Herrmann, H.; Choi, W.; Hoffmann, M. R. *J. Chem. Soc., Faraday Trans.*, in press.

(42) Cordishi, D.; Burriesci, N.; D'Alba, F.; Petrera, M.; Polizzotti, G.; Schiavello, M. *J. Solid State Chem.* **1985**, *56*, 182.

(43) Huheey, J. E. *Inorganic Chemistry; Principles of Structure and Reactivity*; Harper & Row: New York, 1983; pp 73–76.

JP941811Q